ISBN: 978-3-95450-132-8 doi:10.18429/JACoW-IPAC2014-MOPRI046

THE EVOLUTION OF THE TRANSVERSE ENERGY DISTRIBUTION OF ELECTRONS FROM A GaAs PHOTOCATHODE AS A FUNCTION OF ITS DEGRADATION STATE

L.B. Jones*, B.L. Militsyn, T.C.Q. Noakes
STFC Daresbury Laboratory, ASTeC & the Cockcroft Institute, Warrington WA4 4AD, UK
H.E. Scheibler, A.S. Terekhov
Institute of Semiconductor Physics (ISP), SB RAS, Novosibirsk 630090, Russia

Abstract

The brightness of a photoelectron injector is fundamentally limited by the mean longitudinal and transverse energy distributions of the photoelectrons emitted from its photocathode, and the electron beam brightness is increased significantly if the mean values of these quantities are reduced. ASTeC have commissioned a *Transverse Energy Spread Spectrometer* (TESS – an experimental facility designed to measure these transverse and longitudinal energy distributions) which can be used for III-V semiconductor, alkali antimonide/telluride and metal photocathode research [1]. GaAs photocathodes were activated in our photocathode preparation facility (PPF) [2, 3], then transferred to TESS under XHV conditions and progressively degraded through controlled exposure to oxygen. We present commissioning data and initial measurements showing the evolution of the transverse energy distribution of electrons from GaAs photocathodes as a function of their degradation state.

INTRODUCTION

The development of high–performance accelerator drivers for Free–Electron Laser facilities requires electron source technology which delivers a high–brightness electron beam for reasons that are well–documented [4]. Electron beam brightness in an accelerator is fundamentally limited by injector brightness, and this is itself limited by the source beam emittance or the *intrinsic emittance* of the cathode source. Electron beam brightness will be increased significantly by reducing the longitudinal and transverse energy spread in the emitted electrons, thereby creating a *cold beam*.

For a bound electron, the component of electron momentum which is parallel to the cathode surface translates into its transverse momentum component on photoemission. This transverse momentum component is directly related to transverse energy once the electron has been emitted from the cathode, and is measurable as the beam emittance at some distance from the source. When using GaAs photocathodes, the upper limit on transverse electron energy is determined by the illumination wavelength, the level of electron affinity and the photocathode temperature. The profile of the measured transverse energy distribution curve (TEDC) itself depends on various elastic and inelastic electron scattering processes at the photocathode–vacuum interface, which are themselves dependent on a number of factors such as surface roughness, surface diffraction, material structure/crystallinity etc.

The TESS system provides the ability to measure this transverse energy, and to make direct comparisons between photocathodes which have been prepared in different ways or experienced different conditions during operation. This equipment is therefore a key enabling step towards increasing electron beam brightness for future accelerator facilities.

TRANSVERSE ENERGY MEASUREMENT

Work published circa 1972 suggested that the angular size of the photoelectron emission cone from GaAs is small, and this was attributed to photoelectron refraction at the surface–vacuum interface. However, later work appeared to imply the opposite was true [5], the initial results having been distorted by an inhomogenous electric field around the photocathode source arising due to a number of factors such as differences in the work function of the photocathode and its holder. Consequently, the application of angle–resolved photoelectron spectroscopy to measure this angular distribution is challenging as the angular distribution is affected by the specific geometry of the vacuum chamber and experiment itself, so measurements will vary in each installation. Further recent work indicates that the GaAs emission cone is indeed narrow with a half–angle of only 15 ° [6].

It is not possible to decouple the electron transverse energy component from its emission angle when considering only its transverse displacement in the emission plane from the point of emission, and the adverse effects of inhomogenous electric fields and stray magnetic fields on low–energy electrons (typically in the 50 to several hundred eV regime) within the experiment cannot be subtracted. Consequently, data from the TESS includes a contribution from the emission angle, and values returned from a TESS measurement place an upper limit on the mean transverse energy (MTE).

Instrument Description

The TESS system shown in Fig. 1 combines a reflection–mode photocathode holder under grazing–incidence illumination with a retarding–field electron detector and imaging system. The photocathode holder can be electrically biased, and can also be cryogenically–cooled to liquid nitrogen temperature. The source and detector have been designed to be

* lee.jones@stfc.ac.uk

Content from this work may be used under the terms of the CC BY 3.0 licence (© 2014). Any distribution of this work must maintain attribution to the author(s), title of the work, publisher, and DOI.

ISBN: 978-3-95450-132-8 doi:10.18429/JACoW-IPAC2014-MOPRI046

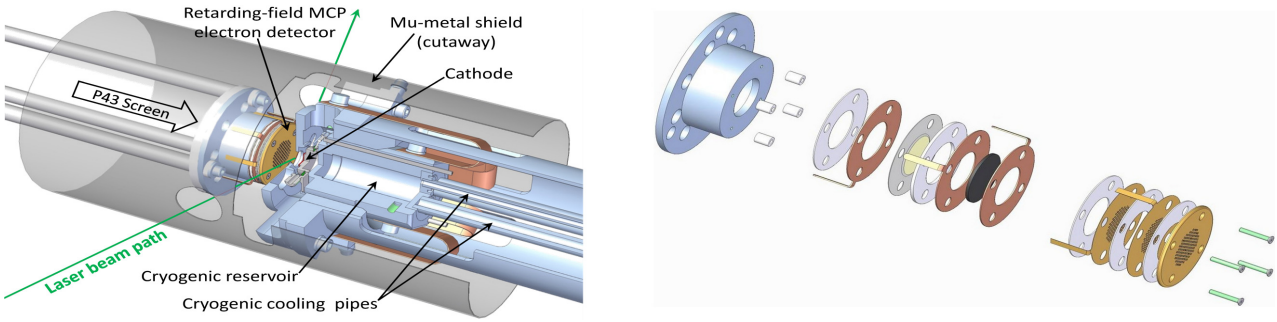

Figure 1: Detail of the TESS experimental system. **Left:** Overview with the vacuum chamber removed and the mu–metal magnetic shield and cathode holder cut away to aid clarity. The cathode holder is shown to the right, the detector to the left. **Right:** Schematic showing an exploded view of the retarding–field electron detector.

symmetric and flat, and contain non–magnetic components. The addition of a mu–metal shield around the source and detector screen against external magnetic fields.

The electron detector shown in Fig. 1 (right) combines three electrically isolated grids with a Hamamatsu F1094-01 2-stage microchannel plate electron multiplier (MCP) and a phosphor screen. The grids are photo–etched from tungsten sheet 35 μm in thickness creating a mesh of pitch 500 μm, then gold–coated to produce non–magnetic assemblies with high electrical conductivity. They are aligned within the detector such that their X- and Y- axes are coincident, and each grid is electrically isolated to 1 kV. Grid #1 and the detector front plate are mechanically flat and electrically common, thereby creating a flat electrical field in the drift space between the source and detector. The MCP front can be earthed or biased, and has an active area 20 mm ϕ. The front–back voltage limit is 2 kV which provides a gain approaching 10^7. The phosphor screen is a P43 ITO type (Gd_2O_2S:Tb), 10 to 15 μm thick with its peak emission at 543 nm, operable at up to 6 kV. Hamamatsu quote a spatial resolution of 80 to 100 μm for this MCP and screen combination. The detector assembly is mounted on a Z–translation stage allowing the electron drift distance between the photocathode source and grid #1 to be varied from a minimum around 7.5 mm to a maximum of 50 mm.

The laser table supports a range of diode lasers at different wavelengths. Several optical elements are used to generate a tightly–focused laser beam and deliver this to the photocathode in grazing–incidence at an angle of 19° wrt the surface plane. Beam profiles measured with a diagnostic camera placed at the equivalent working distance show a beam size around 40 to 80 μm FWHM at the photocathode surface. A series of ND filters are used to control beam intensity.

A PCO.2000 CCD camera captures images from the phosphor screen. The camera has a cooled 2048 × 2048 pixel array with a *Q.E.* (quantum efficiency) around 50 % at 543 nm. It boasts excellent low–noise performance, and has a 14-bit ADC giving a claimed dynamic range of 73 db (around 4,400:1 in practice). Imaging is achieved using a Tamron f 3.5 180 mm macro lens coupled to a Nikon ×2 converter to boost magnification. This combination delivers a spatial resolution of 11 μm/pixel in the recorded images.

Experimental Details - Commissioning

Experiments were performed on p^+-GaAs(100) photocathodes supplied by the ISP and activated in the PPF following established procedures [7, 8], achieving about 2 % quantum efficiency at 635 nm. Once loaded into TESS, it was illuminated with CW laser light at wavelengths of 635 nm and 532 nm. Prior to measurements, the laser power delivered to the cathode was adjusted using ND filters to establish a drain current from the photocathode around 10 pA. During measurements, additional ND filters were inserted increasing beam attenuation by 10^4 and pushing the extracted current to the 1 fA regime, thereby avoiding space–charge effects.

Data was taken with the source at both - 30 V and - 200 V. The detector grids and the MCP front plate were all held at + 30 V. Changing the source voltage controls the accelerating potential (U_{acc}), and therefore the electron time of flight (τ) – the longer flight time associated with a low accelerating voltage gives more time for the transverse energy component to act and thereby expand the emission footprint.

The MCP back plate was held at + 950 V, and the phosphor screen at + 3.5 kV. Screen images showing the electron emission footprint were acquired using camera exposures of 40 s, with extraneous light removed as far as possible. Emission and dark background images were taken in each case, and the dark image then subtracted to create a true image of the emission footprint. Four emission footprint images were measured, corresponding to the two different source voltages and the two different illumination wavelengths. Fig. 2 shows the beam footprints under illumination at λ = 635 nm.

Experimental Details - Degradation

Initial degradation experiments carried out with TESS again use low-efficiency PEA photocathodes with *Q.E.* around 3.5 - 4.0 % under illumination at 635 nm. The higher cathode efficiency necessitated a lower MCP back plate voltage of 900 V. Grid 1 of the detector was held at +20 V, with grids 2, 3 and MCP front held at 0 V. The cathode was operated at -180 V, such that U_{acc} = 200 V. Oxygen was admitted to the TESS chamber at a very low rate using a piezo–electric leak valve, and the chamber pressure monitored to express the integrated exposure in Langmuirs.

Content from this work may be used under the terms of the CC BY 3.0 licence (© 2014). Any distribution of this work must maintain attribution to the author(s), title of the work, publisher, and DOI.

ISBN: 978-3-95450-132-8 doi:10.18429/JACoW-IPAC2014-MOPRI046

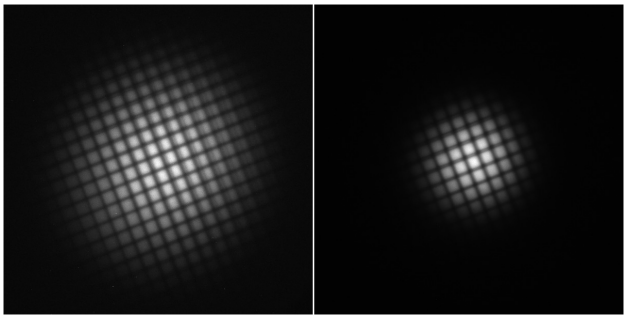

Figure 2: Electron emission footprint under illumination at $\lambda = 635$ nm with the retarding grid structure super–imposed for $U_{acc} = 60$ V (**left**); and $U_{acc} = 230$ V (**right**).

Data Analysis

With the background image subtracted, X- and Y- histograms of the true image were generated which summed each row and column in the data set. Analysis of the histograms was then applied to establish the image centroid, and a radial distribution function $I(r)$ was derived. The function $I(r)$ reflects the number of electrons incident in the annulus with radius r and thickness δr, with the radial displacement r of an electron from the image centroid (where $r = 0$) being dependent on its transverse energy ε_{tr}.

The drift distance between the source and the detector was 43 mm, and the longitudinal accelerating potentials used were $U_{acc} = 60$ V and 230 V respectively during commissioning, and $U_{acc} = 200$ V during the degradation study. In all cases, $e \cdot U_{acc} \gg \varepsilon_{lon}$, so the effect of longitudinal energy content at the instant of emission can be ignored as this will have a negligible effect on the overall flight time. TEDC were calculated for each data set by converting the radial distribution function $I(r)$ to an energy distribution function $N(\varepsilon_{tr})$ based on the radial displacement from the central emission point during the calculated flight time between the source and detector. These were then normalised.

Results

The TEDCs are shown in Fig. 3. The curves have an exponential character, so the values of MTE were extracted by fitting a curve of the form $y = A \times \exp(-\frac{\varepsilon_{tr}}{B})$, where A is the peak intensity and B is the MTE at the $\frac{1}{e}$ level.

The results indicate that the MTE of electrons emitted from a GaAs photocathode is $\text{MTE}_{635} = 45 \pm 7$ meV under illumination at 635 nm, rising to $\text{MTE}_{532} = 100 \pm 15$ meV under illumination at 532 nm. Our results are in good agreement with published measurements [9, 10].

In both cases, the MTEs exceed kT (around 25 meV at room temperature) due to significant contributions from 'hot' non–thermalised electrons. The magnitude of this effect is dependent on illumination wavelength, and Fig. 3 clearly shows that the MTE increases dramatically when the incident photon energy was increased. These experiments were carried out consecutively, so the degradation state of the photocathode was essentially the same in both cases, though the

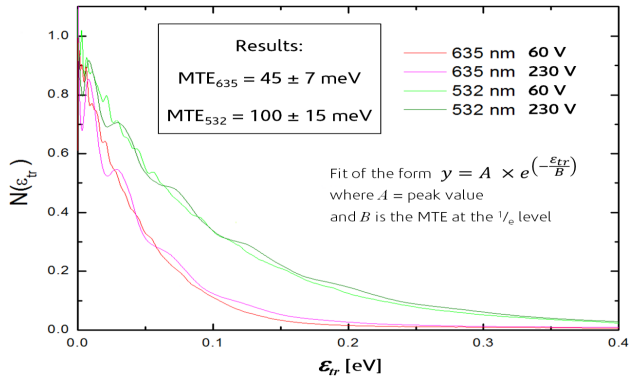

Figure 3: Measurements of transverse energy distribution curve and corresponding MTE for photoelectrons emitted from GaAs under illumination by red and green laser light.

Q.E. will differ according to wavelength. For the 635 nm red laser, $h\nu = 1.95$ eV, rising to $h\nu = 2.33$ eV for the 532 nm green laser. The additional photon energy at 532 nm increases the upper limit on transverse and longitudinal energy for photoemitted electrons, thereby increasing the MTE.

Results from the initial degradation experiment are shown in Fig. 4, and indicate that for this low–efficiency cathode, the MTE is effectively constant with the fitted curves overlapping to ±12 meV, irrespective of degradation state.

FUTURE WORK

A theoretical model of the TESS has been developed by the University of Liverpool [11], and is being refined. This will be used to explore the effects of angular source distribution and field inhomogeneity on the measured results.

New GaAs photocathodes have been loaded into the PPF, and a series of controlled degradation experiments will be carried out using NEA photocathodes over a range of illumination wavelengths. We will also investigate the effects of surface roughening and poor cathode preparation on MTE.

A vacuum suitcase is planned for characterisation of metal photocathodes at room and cryogenic temperatures in TESS, while also giving access to AFM, SEM, XPS and LEED to study photocathode surfaces in detail.

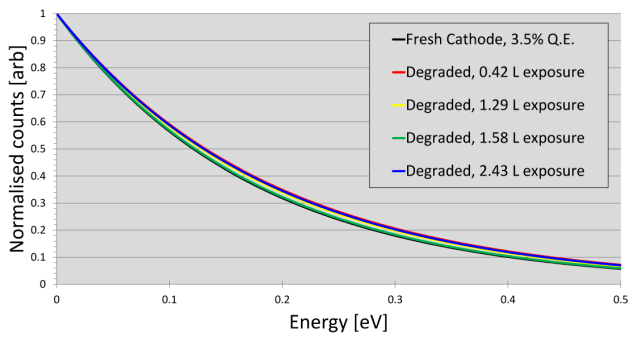

Figure 4: Measurements of the transverse energy distribution curve during photocathode degradation for photoelectrons emitted from GaAs under illumination at 532 nm.

Content from this work may be used under the terms of the CC BY 3.0 licence (© 2014). Any distribution of this work must maintain attribution to the author(s), title of the work, publisher, and DOI.

ISBN: 978-3-95450-132-8 doi:10.18429/JACoW-IPAC2014-MOPRI046

Content from this work may be used under the terms of the CC BY 3.0 licence (© 2014). Any distribution of this work must maintain attribution to the author(s), title of the work, publisher, and DOI.

REFERENCES

[1] L.B. Jones, K.J. Middleman, B.L. Militsyn, T.C.Q. Noakes, D.V. Gorshkov, H.E. Scheibler & A.S. Terekhov, Proc. FEL2013, TUPS033, 290-293.

[2] B.L. Militsyn, I. Burrows, R.J. Cash, B.D. Fell, L.B. Jones, J.W. McKenzie, K.J. Middleman, H.E. Scheibler & A.S. Terekhov, IPAC'10, TUPE095, pages 2347-2349.

[3] L.B. Jones, R.J. Cash, N. Chanlek, B.D. Fell, J.W. McKenzie, K.J. Middleman & B.L. Militsyn; Proc. IPAC '11, 3185-87.

[4] D.H. Dowell, I.V. Bazarov, B.M. Dunham, K.Harkay, C. Hernandez-Garcia, R. Legg, H. Padmore, T. Rao, J. Smedley & W. Wan; NIM 'A' 622 (2010), 685–697.

[5] D.J. Bradley, M.B. Allenson & B.R. Holeman; J. Phys. D.: Appl. Phys. 10(1), 1977, 111-125.

[6] Z. Liu, Y. Sun, P. Pianetta & R.F.W. Pease; J. Vac. Sci. Technol. B 23(6), 2005, 2758-2762.

[7] W.E. Spicer & R.L. Bell; Pub. Astron. Soc. **84** 110 (1972).

[8] W.E. Spicer, Appl. Phys. **12**, 115 (1977).

[9] I.V. Bazarov, B.M. Dunham, F. Hannon, Y. Li, X. Liu, T. Miyajima, D.G. Ouzounov & C.K. Sinclair; Proc. PAC '07, 1221-1223.

[10] S. Matsuba, Y. Honda, X. Jin, T. Miyajima, M. Yamamoto, T. Uchiyama, M. Kuwahara & Y. Takeda; Jap. J. Appl. Phys. 51 (2012), 046402.

[11] L.J. Devlin, O. Karamyshev, C.P. Welsch, L.B. Jones, B.L. Militsyn & T.C.Q. Noakes; IPAC '14, MOPRI051, these proceedings.